Chimica Techno Acta
published by Ural Federal University
eISSN 2411-1414
chimicatechnoacta.ru

ARTICLE
2024, vol. 11(3), No. 202411305
DOI: 10.15826/chimtech.2024.11.3.05

Methyl orange sorption on octadecylamine-modified iron oxide magnetic nanoparticles

Liang Tianhui [ab], Sayara Aga-Tagieva [b], Alexander Omelyanchik [b], Zhang Xiaozhou [a], Hong Lu [a], Katerina Levada [b], Valeria Rodionova [b], Kurban Magomedov [bc] *

a: College of Material Science and Engineering, Qiqihar University, Qiqihar, 161006, China
b: REC "Smart Materials and Biomedical Application, I. Kant Baltic Federal University, Kaliningrad 236001, Russia
c: Department of Analytical and Pharmaceutical Chemistry, Dagestan State University, Makhachkala, 367000, Russia
* Corresponding author: m_kurban@mail.ru

This paper belongs to a Regular Issue.

Abstract

This study investigates the sorption of 2-methyl orange dye onto octadecylamine-modified iron oxide magnetic nanoparticles (ODA-IONPs). The synthesized ODA-IONPs exhibit remarkable sorption capacity, reaching 800 mg/g at the nanoparticle concentrations ranging from 5 to 10 mg/g and pH of 2–8. The sorption process demonstrates rapid kinetics, achieving 90% of maximum sorption within 0.5 min. Thermodynamic analysis showed that sorption process is spontaneous and endothermic, as indicated by negative ΔG and positive ΔH values. The pseudo-second-order and Langmuir models best describe the sorption kinetics at 293 K ($R^2 > 0.99$). Compared to other adsorbents, ODA-IONPs show superior MO removal capacity under a wider pH range. The influence of nanoparticle concentration, pH, and temperature on sorption efficiency is systematically explored, with optimal conditions identified at 10 mg/L ODA-IONPs and pH 6. Furthermore, the feasibility of nanoparticle reusability for sorption purposes is assessed. These findings underscore the potential of ODA-IONPs as efficient sorbents for wastewater treatment and environmental remediation applications.

Keywords

sorption
methyl orange
magnetic nanoparticles
octadecylamine
kinetics
thermodynamics
Fe_3O_4

Received: 04.06.24
Revised: 04.07.24
Accepted: 11.07.24
Available online: 22.07.24

Key findings

- The adsorption capacity of ODA-IONPs was highest at 5 mg/L and 10 mg/L concentrations.
- The sorption process was spontaneous and endothermic, with negative ΔG values and a positive ΔH value.
- The pseudo-second-order and Langmuir models best described the dye sorption on ODA-IONPs at 293 K.

1. Introduction

During the process of modern industrial development, the usage of colored materials and dyes is indispensable, especially in industries such as textiles, food, and plastics [1, 2]. 2-Methyl Orange (MO), a simple and stable dye, is economically viable and resistant to decomposition under ultraviolet radiation. It constitutes approximately half of the dyes used in the textile industry and finds wide application in textile dyeing. However, MO itself is a toxic and harmful substance that can cause irritation to the human body. Prolonged exposure to MO can potentially lead to reproductive system and liver toxicity issues [3,4]. In industrial wastewater, if MO is discharged untreated directly into water sources and soil, it generates a large amount of suspended dye molecules, severely impacting the transparency of water bodies and affecting the life activities of fish, plants, and microorganisms. This poses serious threats to local ecosystems and food chains. Additionally, MO can be released into the air, causing negative impacts on air quality and atmospheric environment [5–8]. Therefore, it is essential to treat industrial wastewater containing MO before its discharge to ensure safety and harmlessness.

Currently, methods for treating dye wastewater can be categorized into physical, biological, conventional chemical, and advanced oxidation processes [9]. Among these methods, physical processes such as adsorption [10], membrane separation [11], and ion exchange[12] are commonly used techniques for treating dye-polluted wastewater [13]. Biological processes utilize the metabolic processes of microorganisms such as bacteria and fungi to decompose organic pollutants in wastewater and purify the sewage, including aerobic biological processes [14], anaerobic biological processes [15], and aerobic/anaerobic mixed processes [16, 17]. They have advantages such as low cost and large treatment range. However, these processes have several limitations for environmental treatment, requiring suitable temperature, light, pH, and oxygen concentrations. In practical wastewater treatment, the complex water quality may result in insufficient biodegradability and low degradation performance for dye-containing wastewater [18]. Conventional chemical processes, such as electrochemical methods [19], chemical precipitation [20], redox reactions, and coagulation [21, 22] alter the physical or chemical properties of pollutants in wastewater to change their forms, causing them to precipitate, float, or be partitioned into small molecular states. However, these methods are often associated with high costs, high energy consumption, and the need for complex post-treatment processes to avoid secondary pollution of the environment [23]. Advanced oxidation processes, which involve reactions under conditions of light [24], catalysts, high temperature, and high pressure, can degrade pollutants into small molecular substances and purify wastewater. However, their effectiveness in handling pollutants with high organic content is not ideal [25, 26].

Adsorption is a physical purification method that utilizes the porous physical properties of adsorbents to adsorb organic dyes from wastewater onto the surface or within the pores, thereby physically separating them from the wastewater. It has such advantages as simplicity, high efficiency, no pollution, and economic viability, making it an excellent method for purifying dye wastewater and the optimal and comprehensive technique for removing azo dyes from water [27]. There are many types of adsorbents available, among which activated carbon [28, 29], due to its microporous structure, large surface area, and strong adsorption capacity, is widely used. However, it has the drawbacks of high production costs and poor recycling performance. Various low-cost adsorbents such as alumina [30], zeolite [31, 32], polymers [33], activated carbon [34], silica [35], gel chitosan, clay materials [36], and agricultural [37] and industrial wastes [38, 39] have been extensively employed [40, 41]. However, research has shown that these low-cost adsorbents do not possess sufficient adsorption performance for MO [42, 43].

Iron oxide nanoparticles (IONPs), specifically those based on γ-Fe_2O_3 and Fe_3O_4, have rapidly advanced for sorption application owing to their magnetic properties, enabling their efficient collection with a magnetic field [44]. Their biocompatibility, ease of preparation, and high extraction efficiency enhance their effectiveness in solid-liquid separation, making them valuable adsorbents for water purification and various other applications[45–48]. The preparation methods for γ-Fe_2O_3/Fe_3O_4 IONPs include co-precipitation [49–51], microemulsion [52], thermal decomposition [53], and hydrothermal synthesis [54]. The co-precipitation method not only stands out for its simplicity and efficacy in the synthesis of IONPs but also offers an eco-friendly advantage by circumventing the use of toxic reagents [55].

However, bare IONPs have a tendency to self-aggregate and minimize their surface energy. To ensure chemical stability and uniform particle size of IONPs, protective coatings can be applied to the surface, which effectively increases the surface area-to-volume ratio of the particles [48, 56, 57]. Surface modification with various molecules, such as propylene glycol, silane coupling agents, citric acid, and hexadecyltrimethylammonium bromide [58, 59], can be used to meet different requirements. Moreover, different reactive groups, such as epoxy, carbonyl, and carboxyl groups, can be introduced onto IONPs through chemical reactions, enabling chemical bonding, π-π stacking, ion binding, and hydrogen bonding [60, 61].

In this study, the co-precipitation method was used to synthesize magnetic IONPs coated with octadecylamine (ODA). This ODA-IONPs composite was tested for adsorption capacity of MO under different conditions, and their adsorption kinetics was thoroughly studied to determine the optimal parameters and mechanical models for improving the efficiency of the process.

2. Experimental

2.1. Chemicals, materials and equipment

Iron (III) chloride hexahydrate ($FeCl_3 \cdot 6H_2O$, ≥98%, LenReaktiv), Iron(II) sulfate heptahydrate ($FeSO_4 \cdot 7H_2O$, ≥98%, LenReaktiv), sodium hydroxide (NaOH, ≥98%, Sigma-Aldrich) and octadecylamine ($C_{18}H_{39}N$, ≥98%,LenReaktiv) were used for the synthesis of the IONPs, MO ($C_{14}H_{14}N_3O_3SNa$, ≥99%, pure for analysis, LenReaktiv). Absorption spectra were measured with a spectrophotometer SF-2000 (Manufacturer: OKB Spektr, St. Petersburg) in the wavelength range from 200 to 800 nm with a scanning step of 0.1 nm and a slit width of 1 nm.

2.2. Nanoparticle preparation

IONPs were synthesized by co-precipitation method as described elsewhere [49–51] with some modifications. Solutions of Fe^{2+} (10 mL, 10 mmol/L) and Fe^{3+} (10 mL, 20 mmol/L) were prepared in distilled water preheated to 80 °C. Sodium hydroxide solution (30 mmol/L) was then incrementally added under vigorous stirring to adjust the pH to value within the range of 9.0 to 11.0. The reaction mixture was maintained at 80 °C for 2 h with continuous stirring. Afterwards, the mixture was allowed to cool to

 DOI: 10.15826/chimtech.2024.11.3.05

room temperature, and the resultant black precipitate was separated using permanent magnets (with the induction of magnetic field at surface of about 1.2 T). The precipitate was purified by washing twice with distilled water and thrice with ethanol. The purified precipitate was resuspended in 250 mL of distilled water. Separately, 1 g of ODA was dissolved in 250 mL of acetone, and this solution was added to the aqueous suspension. The mixture was stirred for 24 h at 30 °C, resulting in the synthesis of ODA-modified iron oxide (γ-Fe_2O_3/Fe_3O_4) nanoparticles (ODA-IONPs).

As we demonstrated earlier [62], the obtained particles were approximately 8 nm in size according to Transmission Electron Microscopy (TEM). X-ray Diffraction (XRD) analysis revealed that they possess a spinel ferrite structure typical for both magnetic iron oxides γ-Fe_2O_3 and Fe_3O_4. The synthesized particles showed superparamagnetic behavior at room temperature with saturation magnetization of approximately 55 Am^2/kg, which is consistent with the expectations for nanoparticles of this size [50, 51].

2.3. Sorption study

2.3.1. Capacity

To determine the sorption capacity, a solution of ODA-IONPs (100 mg/l, 5 ml) was added to a MO solution (100 mg/l, 5 ml). The pH was adjusted to the desired level using hydrochloric acid and sodium hydroxide. Distilled water was then added to bring the volume to 50 ml, and the pH value was measured again to confirm the acidity. The solutions were placed on a stirrer for 1 h. After this period, the optical density of the solution was measured, followed by the magnetic separation and filtration steps. The optical density was recorded at a wavelength of 469 nm and compared with the calibration curve to determine the concentration of MO.

The static capacity of the adsorbent ODA-IONPs was calculated using the following formula:

$$q_t = \frac{(C_0 - C_{eq})V}{m} \quad (1)$$

where C_0 is the initial concentration of the dye, C_{eq} is the equilibrium concentration of the dye, V is the volume of the flask, and m is the mass of the sorbent.

2.3.2. Effect of IONPs concentration on degree of extraction

The effect of a samples weight was studied in a manner similar to the one used for the pH, but using the optimum values of acidity, pH 6–8. The weight varied from 50 to 200 mg. The degree of extraction was calculated with the formula:

$$R = \frac{(C_0 - C_{eq})}{C_{eq}}\ 100\%. \quad (2)$$

2.3.3. Period of sorption

To assess the period of sorption, distilled water was added to a 100 ml flask containing ODA-IONPs solution (100 mg/l, 10 ml) and MO solution (100 mg/l, 10ml) to the labeled mark. The flask was then put on a stirrer. The optical density measurements of the solution were taken by collecting 3.5 ml samples after 0.5, 1.5, 3.5, 5, 10, 20, 30, 40, 50, 60, 90, and 120 min.

2.3.4. Kinetics of sorption

The kinetics of MO adsorption on IONPs samples modified with ODA was analyzed using pseudo-first-order [63], second-order [64], Elovich [65, 66], Weber and Morris model [67], Langmuir [68], Freundlich [69], Temkin [70] and Dubinin–Radushkevich [71] models, which can be expressed in linear form as

$$\ln(q_e - q_t) = \ln q_e - k_1 t, \quad (3)$$

where q_e and q_t (mg/g) are the amount of adsorbed MO at equilibrium and at time t, respectively; k_1 is the equilibrium rate constant in the pseudo-first-order model (L/min);

$$\frac{t}{q_t} = \frac{1}{k_2 q_e^2} + \frac{1}{q_e} t, \quad (4)$$

where q_e is the amount of the dye adsorbed at equilibrium (mg/g), and k_2 is the equilibrium rate constant of the pseudo-second-order model (g/mg min);

$$q_t = \frac{1}{\beta}\ln(\alpha\beta) + \frac{1}{\beta}\ln t, \quad (5)$$

where α is the initial adsorption rate and β is the desorption constant;

$$q_t = k_i t^{0.5} + C_p, \quad (6)$$

$$\frac{C_p}{q_t} = \frac{1}{q_e k_L} + \frac{1}{q_e} C_p, \quad (7)$$

$$\ln q_t = \ln k_F + \frac{1}{n} C_p, \quad (8)$$

$$q_t = B \ln k_T + B \ln C_p, \quad (9)$$

$$\ln q_t = \ln q_{D-R} - k_{D-R}\epsilon^2, \quad (10)$$

where k_i, k_L, k_F, k_T, and $k_{D\text{-}R}$, are the intraparticle diffusion rates (mg/g $min^{-0.5}$) according to the Weber and Morris, Langmuir, Freundlich, Temkin, Dubinin–Radushkevich models, respectively; t, C_p is a constant for any experiment (mg/dm^3), n is the Freundlich isotherm constant, showing the heterogeneity of the surface, B is the constant associated with the heat of sorption (J/mol), $q_{D\text{-}R}$ is the theoretical capacity of the sorbent (mol/g); ϵ is the Polyani potential.

3. Results and Discussion

Figure 1 illustrates the effect of different concentrations (0.5–100 mg/l) of ODA-IONPs on the adsorption process of 10 mg/l MO solution. The adsorption capacity (q) and separation factor (R) were measured after adsorption for 2 h. The q value increased gradually, reaching a maximum of 768.6 mg/g at a concentration of 5 mg/L, after which it gradually decreased. R gradually increased in the range of

 DOI: 10.15826/chimtech.2024.11.3.05

0–10 mg/l, then decreased in the range of 10–100 mg/l, achieving a maximum of 95% at 100 mg/l ODA-IONPs.

Through comparison and selection of the above results, it was found that the q of ODA-IONPs reached its highest values at the concentrations of 5 mg/l and 10 mg/l, while R was highest at the concentration of 10 mg/l. Therefore, the concentration of 10 mg/L is considered to be the optimal adsorption concentration for ODA-IONPs. This concentration provides the best balance between high adsorption capacity and efficient separation of the MO dye from the solution.

Figure 2 lists the effects of different PH environments on the adsorption of ODA-IONPs. The concentrations of ODA-IONPs and MO are both 10 mg/l. At room temperature, with the increase of pH value, q and R both increase first and then decrease, reaching the highest values at pH ~6.0. This phenomenon can be attributed to the behavior of ODA-IONPs at different concentrations. At low concentrations (10 mg/L and below), the ODA-IONPs remain well-dispersed without significant agglomeration. However, as the concentration increases (20 mg/L and above), the zeta potential decreases, leading to nanoparticle agglomeration. This agglomeration reduces the effective surface area available for interaction with MO molecules. Consequently, the contact area between the ODA-IONPs and MO decreases, resulting in a lower sorption capacity of the sorbent.

Figure 3 shows the effects of different reaction temperature and time on the adsorption q value of ODA-IONPs at the reaction temperatures of 293, 303, 313 and 323 K, respectively, while both ODA-IONPs and MO concentrations of ODA-IONPs and MO are set at 10 mg/l and a pH of 6.0. The q value was observed to increase with time, and higher reaction temperatures resulted in higher q values. Compared with the four reaction temperature curves, the q value increases greatly from 293 to 303 K, while the three curves at 303, 313 and 323 K have little difference. Table 1 presents the time for reaching the highest q value at the four reaction temperatures, as well as the time for reaching 95% ($t_{95\%}$) and 90% ($t_{90\%}$) of the highest q value. It can be seen from the figure that the highest q value at the four reaction temperatures is reached at 120 min. Within the range of 293–313 K, it only takes 0.5 min to reach 90% of the highest q value. At 323 K, only 0.5 min is needed to achieve 95% of the maximum q value.

Figure 4 illustrates the effects of different reaction temperatures and time on the adsorption R value of ODA-IONPs. The trends observed in R values were consistent with those for q in Figure 3. As the reaction temperature increased, the R value also increased, indicating enhanced adsorption efficiency at higher temperatures.

The Gibbs energy (ΔG) values at all indicated temperatures are negative, which indicates the spontaneity of the sorption process. With increasing temperature, the ΔG values become more negative, which indicates an increase in the spontaneity of the sorption process with increasing temperature.

Table 1 Temperature dependence of the time to reach different degrees of sorption and the amount of adsorbed MO.

T, K	$t_{100\%}$, min (q, mg/g)	$t_{95\%}$, min (q, mg/g)	$t_{90\%}$, min (q, mg/g)
293	120 (926.4)	5 (880.0)	0.5 (837.71)
303	120 (968.6)	5 (920.1)	0.5 (871.70)
313	120 (959.4)	1.5 (911.4)	0.5 (835.37)
323	120 (967.8)	0.5(919.4)	

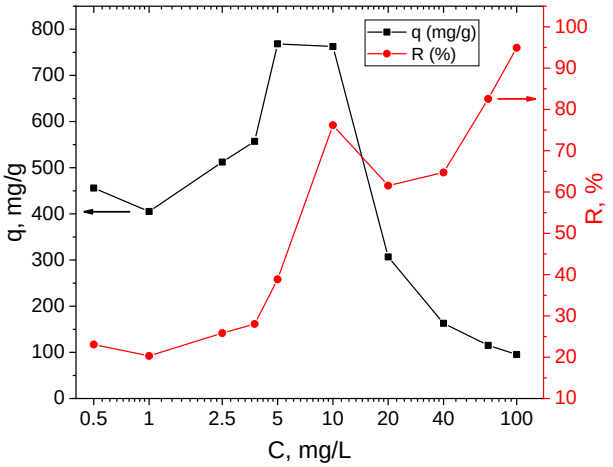

Figure 1 Dependence of the sorption and degree of sorption of MO on ODA-modified iron oxide magnetic nanoparticles on the different concentrations of ODA-IONPs.

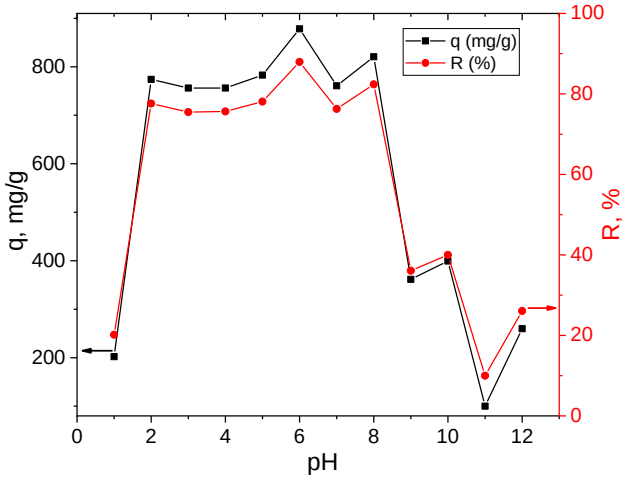

Figure 2 Dependence of the sorption and degree of sorption of MO on ODA-IONPs vs pH.

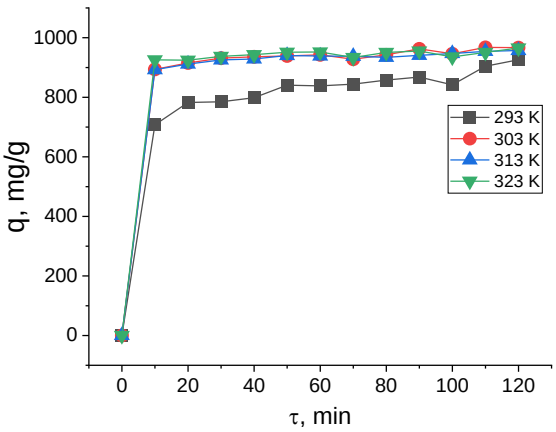

Figure 3 Dependence of degree of sorption of MO on the ODA-IONPs from time at different temperatures.

 DOI: 10.15826/chimtech.2024.11.3.05

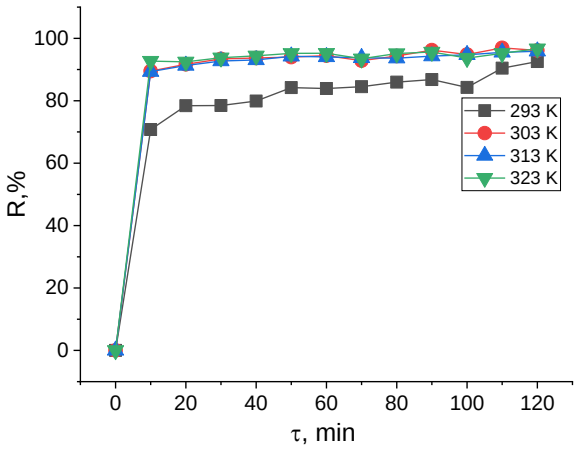

Figure 4 Dependence of degree of sorption of MO on ODA-IONPs on time at different temperatures.

The positive entropy change (ΔS = 164.64 J/(mol·K)) indicates an increase in the entropy of the system during sorption, likely due to the increased disorder or mobility of dye molecules on the surface of nanoparticles. A positive enthalpy (ΔH = 43.4 kJ/mol) indicates that the sorption process is endothermic, requiring the absorption of heat from the environment. Thus, the process of dye sorption on nanoparticles is spontaneous and endothermic, accompanied by a decrease in the entropy of the system. An increase in temperature contributes to an increase in the spontaneity of the process, which manifests itself in more negative ΔG values.

From the analysis of Table 2, it can be seen that the pseudo-second-order and Langmuir models most accurately describe the dye sorption on ODA-ONPs at 293 K. These models have high coefficients of determination (R^2), indicating good agreement with the experimental data. The negative values of ΔG by Langmuir model confirm the spontaneous nature of the sorption process. The Freundlich, Temkin and Dubinin–Radushkevich models also show relatively high values of R^2, but with some anomalies in the parameters, which requires further study.

3.1. Comparison with other adsorbents

For further comparison with other various adsorbents, the adsorption capacity (q_{max}; mg/g) of different adsorbents reported in the literature [66, 72, 81, 73–80] are listed in Table 3. According to this Table, the adsorption capacities of the ODA-IONPs were much higher than those of the reported adsorbents, indicating that the ODA-IONPs have important potential for the adsorption MO from aqueous solution. Only magnetic hierarchical porous carbon spheres have higher capacity, but lower pH range (study only for pH 7) [81].

4. Limitations

Difficulties can arise in the determination of dyes at different pH because errors occur when determining the concentration at the isosbestic point. Simple and rapid methods are needed for the determination of various dyes (including MO) in sorption and catalysis studies using CCD spectrophotometers and chemometric processing, possibly using neural networks.

5. Conclusions

The investigation into ODA-IONPs reveals their substantial potential as sorbents for MO dye, with a maximum capacity of 800 mg/g and rapid sorption kinetics with 90% of maximum sorption achieved within 0.5 min. Thermodynamic analysis reveals the process to be spontaneous (ΔG < 0) and endothermic (ΔH = 43.4 kJ/mol). The high adsorption capacity, rapid kinetics, and wide pH range (2–8) of ODA-IONPs offer significant advantages over conventional adsorbents.

Table 2 Parameters of kinetics model for sorption of ODA-IONPs of MO.

Model	Model parameters	*T*, K			
		293	303	313	323
PFO	k_1	$8{\cdot}10^{-5}$	$8{\cdot}10^{-5}$	$8{\cdot}10^{-5}$	$8{\cdot}10^{-5}$
	R^2	0.576	0.7593	0.8606	0.4605
PSO	K_2	0.0011	0.001	0.001	0.001
	R^2	0.9988	0.9998	0.9999	0.9997
Langmuir	R^2	0.9951	0.9992	0.9994	0.9998
	K_L, l/mol	5.1371	24.1973	19.8059	35.1309
	a_{MAX}, mol/g	0.00225	0.00265	0.00262	0.00273
	ΔG, J/mol	−3988.54	−8030.57	−7774.09	−9562.07
Freundlich	R^2	0.8032	0.9535	0.9697	0.9812
	K_F	0.00275	0.00277	0.00276	0.00279
	n	−7.752	−15.823	−13.736	−18.315
Temkin	R^2	0.8084	0.9591	0.9736	0.9829
	K_T	0.000123	$8.31529{\cdot}10^{-7}$	$8.31529{\cdot}10^{-7}$	$8.31529{\cdot}10^{-7}$
	B	−0.0003	−0.0002	−0.0002	−0.0002
Dubinin–Radushkevich	R^2	0.7672	0.9184	0.9433	0.9669
	$K_{D\text{-}R}$	0.0001	0.00004	0.00005	0.00003
	a, mol/g	0.00222	0.00260	0.00255	0.00265

 DOI: 10.15826/chimtech.2024.11.3.05

Table 3 Comparison of MO adsorption capacity of ODA-IONPs with that of various adsorbents.

No.	Adsorbent Material	R, %	q_{Max}, mg/L	pH	Method of q_{Max}	Reference
1	Fe_3O_4@SiO_2	83	182.5	2	Langmuir	[72]
2	Fe_3O_4-CTAB	~90	7.6	4–6	Langmuir	[73]
3	Magnetic hierarchical porous carbon spheres	99.9	1522.6	7	Langmuir	[81]
4	Goethite	91	55	3	Langmuir	[74]
	Chitosan beads	94	73	3	Langmuir	
	Goethite impregnated with chitosan beads	96	84	3	Langmuir	
5	Fe_3O_4/GO nanocomposite	98	714.3	6	Langmuir	[75]
6	Grapheme oxide	98.2	543.4	5	Langmuir	[76]
7	Fe_3O_4@MUS composite	85	149.25	3	Langmuir	[77]
8	MWCNTs/Fe_3O_4/PANI	–	544.99	4	Langmuir	[78]
9	Chitosan Bead-like Materials	98.8	12.46	4–6	Langmuir	[66]
10	Silicate minerals:					[79]
	Halloysite nanotubes	–	13.56	7	Langmuir	
	Chrysotile nanotubes	–	31.46	7	Langmuir	
11	$[Bi_6O_5(OH)_3](NO_3)_5 \cdot 3H_2O$	97	730	6–8	Langmuir	[80]
12	ODA-IONPs	90	880	6	Langmuir	This work
13	ODA-IONPs	80	800	2–8	Langmuir	This work

These properties, combined with their magnetic nature allowing easy separation, position ODA-IONPs as promising candidates for large-scale wastewater treatment applications, particularly in textile and dye industries. Future studies should explore the scalability of ODA-IONPs synthesis and their efficacy against a broader range of pollutants, paving the way for comprehensive environmental remediation strategies.

• Supplementary materials

No supplementary materials are available.

• Conflict of interest

The authors declare no conflict of interest.

• Acknowledgement

None.

• Funding

This work was supported by the Russian Science Foundation; grant no. 22-22-20124, regional part no. 08-C/2022, https://www.rscf.ru/en.

• Author contributions

Conceptualization: K.M.
Data curation: K.M.
Formal Analysis: Z.H., L.H., K.L., V.R.
Funding acquisition: K.L.
Investigation: L.T., S.A.T., K.M.
Methodology: K.M., A.O.
Project administration: K.L., K.M.
Resources: V.R., K.L., K.M.
Supervision: Z.H., L.H., K.L., V.R.
Validation: Z.H., L.H., K.L., V.R.
Visualization: L.T., S.A.T., K.M.
Writing – original draft: L.T., S.A.T., K.M.
Writing – review & editing: A.O., K.L., V.R.

• Additional information

Author IDs:
Liang Tianhui, Scopus ID 57417402100;
Sayara Aga-Tagieva, Scopus ID 58548751300;
Alexander Omelyanchik, Scopus ID 57196416798;
Zhang Xiaozhou, Scopus ID 11639083000;
Hong Lu, Scopus ID 57224814524;
Katerina Levada, Scopus ID 58497273900;
Valeria Rodionova, Scopus ID 7003646285;
Kurban Magomedov, Scopus ID 55992161500.

Websites:
Qiqihar University, https://www.qqhru.edu.cn/;
I. Kant Baltic Federal University, https://kantiana.ru/en/;
Dagestan State University, https://dgu.ru/.

References

1. Lin J, Ye W, Xie M, Seo DH, Luo J, Wan Y, et al. Environmental impacts and remediation of dye-containing wastewater. Nat Rev Earth Environ 2023 411. 2023;4:785–803. doi:10.1038/s43017-023-00489-8
2. Ali K, Zeidan H, Amar B, Ali (K, Zeidan H. Evaluation of the use of agricultural waste materials as low-cost and eco-friendly sorbents to remove dyes from water: a review. 2023 [cited 18 May 2024]. doi:10.5004/dwt.2023.29725
3. Al-Tohamy R, Ali SS, Li F, Okasha KM, Mahmoud YAG, Elsamahy T, et al. A critical review on the treatment of dye-containing wastewater: Ecotoxicological and health concerns of textile dyes and possible remediation approaches for

 DOI: 10.15826/chimtech.2024.11.3.05

environmental safety. Ecotoxicol Environ Saf. 2022;231:113160. Medline:35026583 doi:10.1016/J.ECOENV.2021.113160
4. Jan S, Mishra AK, Bhat MA, Bhat MA, Jan AT. Pollutants in aquatic system: a frontier perspective of emerging threat and strategies to solve the crisis for safe drinking water. Environ Sci Pollut Res Int. 2023;30:113242–79. Medline:37864686 doi:10.1007/S11356-023-30302-4
5. Islam T, Repon MR, Islam T, Sarwar Z, Rahman MM. Impact of textile dyes on health and ecosystem: a review of structure, causes, and potential solutions. Environ Sci Pollut Res 2022 304. 2022;30:9207–42. Medline:36459315 doi:10.1007/S11356-022-24398-3
6. Sehar S, Rasool T, Syed HM, Mir MA, Naz I, Rehman A, et al. Recent advances in biodecolorization and biodegradation of environmental threatening textile finishing dyes. 3 Biotech. 2022;12:1–12. doi:10.1007/S13205-022-03247-7
7. Peramune D, Manatunga DC, Dassanayake RS, Premalal V, Liyanage RN, Gunathilake C, et al. Recent advances in biopolymer-based advanced oxidation processes for dye removal applications: A review. Environ Res. 2022;215:114242. Medline:36067842 doi:10.1016/J.ENVRES.2022.114242
8. Saad I, Ralha N, Abukhadra MR, Al Zoubi W, Ko YG. Recent advances in photocatalytic oxidation techniques for decontamination of water. J Water Process Eng. 2023;52:103572. doi:10.1016/J.JWPE.2023.103572
9. Solayman HM, Hossen MA, Abd Aziz A, Yahya NY, Leong KH, Sim LC, et al. Performance evaluation of dye wastewater treatment technologies: A review. J Environ Chem Eng. 2023;11:109610. doi:10.1016/J.JECE.2023.109610
10. Wang J, Guo X. Adsorption kinetic models: Physical meanings, applications, and solving methods. J Hazard Mater. 2020;390:122156. Medline:32006847 doi:10.1016/J.JHAZMAT.2020.122156
11. Feng X, Peng D, Zhu J, Wang Y, Zhang Y. Recent advances of loose nanofiltration membranes for dye/salt separation. Sep Purif Technol. 2022;285:120228. doi:10.1016/J.SEPPUR.2021.120228
12. Cai L, Ying D, Liang X, Zhu M, Lin X, Xu Q, et al. A novel cationic polyelectrolyte microsphere for ultrafast and ultra-efficient removal of heavy metal ions and dyes. Chem Eng J. 2021;410:128404. doi:10.1016/J.CEJ.2021.128404
13. Ahmed SF, Mofijur M, Nuzhat S, Chowdhury AT, Rafa N, Uddin MA, et al. Recent developments in physical, biological, chemical, and hybrid treatment techniques for removing emerging contaminants from wastewater. J Hazard Mater. 2021;416:125912. doi:10.1016/J.JHAZMAT.2021.125912
14. Khouni I, Marrot B, Amar R Ben. Treatment of reconstituted textile wastewater containing a reactive dye in an aerobic sequencing batch reactor using a novel bacterial consortium. Sep Purif Technol. 2012;87:110–9. doi:10.1016/J.SEPPUR.2011.11.030
15. Türgay O, Ersöz G, Atalay S, Forss J, Welander U. The treatment of azo dyes found in textile industry wastewater by anaerobic biological method and chemical oxidation. Sep Purif Technol. 2011;79:26–33. doi:10.1016/J.SEPPUR.2011.03.007
16. Lin X, Zhou Q, Xu H, Chen H, Xue G. Advances from conventional to biochar enhanced biotreatment of dyeing wastewater: A critical review. Sci Total Environ. 2024;907:167975. doi:10.1016/J.SCITOTENV.2023.167975
17. Kasbaji M, Mennani M, Oubenali M, Ait Benhamou A, Boussetta A, Ablouh EH, et al. Bio-based functionalized adsorptive polymers for sustainable water decontamination: A systematic review of challenges and real-world implementation. Environ Pollut. 2023;335:122349. doi:10.1016/J.ENVPOL.2023.122349
18. Yu JX, Chi RA, He ZY, Qi YF, Zhan G, Guo J. Combination of biosorption and photodegradation to remove methyl orange from aqueous solutions. Eng Life Sci. 2011;11:309–315. doi:10.1002/ELSC.201000158
19. Särkkä H, Bhatnagar A, Sillanpää M. Recent developments of electro-oxidation in water treatment — A review. J Electroanal Chem. 2015;754:46–56. doi:10.1016/J.JELECHEM.2015.06.016
20. Ondersma JW, Hamann TW. Recombination and redox couples in dye-sensitized solar cells. Coord Chem Rev. 2013;257:1533–43. doi:10.1016/J.CCR.2012.09.010
21. Al-Raad AA, Hanafiah MM. Removal of inorganic pollutants using electrocoagulation technology: A review of emerging applications and mechanisms. J Environ Manage. 2021;300:113696. doi:10.1016/j.jenvman.2021.113696
22. Aragaw TA, Bogale FM. Role of coagulation/flocculation as a pretreatment option to reduce colloidal/bio-colloidal fouling in tertiary filtration of textile wastewater: A review and future outlooks. Front Environ Sci. 2023;11:1142227. doi:10.3389/FENVS.2023.1142227/BIBTEX
23. Khan MD, Singh A, Khan MZ, Tabraiz S, Sheikh J. Current perspectives, recent advancements, and efficiencies of various dye-containing wastewater treatment technologies. J Water Process Eng. 2023;53:103579. doi:10.1016/J.JWPE.2023.103579
24. Islam M, Kumar S, Saxena N, Nafees A. Photocatalytic Degradation of Dyes Present in Industrial Effluents: A Review. ChemistrySelect. 2023;8:e202301048. doi:10.1002/SLCT.202301048
25. Ahsan A, Jamil F, Rashad MA, Hussain M, Inayat A, Akhter P, et al. Wastewater from the textile industry: Review of the technologies for wastewater treatment and reuse. Korean J Chem Eng 2023 409. 2023;40:2060–2081. doi:10.1007/S11814-023-1475-2
26. Ledakowicz S, Pázdzior K. Recent Achievements in Dyes Removal Focused on Advanced Oxidation Processes Integrated with Biological Methods. Mol 2021, Vol 26, Page 870. 2021;26:870. doi:10.3390/MOLECULES26040870
27. Darwish AAA, Rashad M, AL-Aoh HA. Methyl orange adsorption comparison on nanoparticles: Isotherm, kinetics, and thermodynamic studies. Dye Pigment. 2019;160:563–71. doi:10.1016/J.DYEPIG.2018.08.045
28. Jorge AMS, Athira KK, Alves MB, Gardas RL, Pereira JFB. Textile dyes effluents: A current scenario and the use of aqueous biphasic systems for the recovery of dyes. J Water Process Eng. 2023;55:104125. doi:10.1016/J.JWPE.2023.104125
29. Kumar N, Pandey A, Rosy, Sharma YC. A review on sustainable mesoporous activated carbon as adsorbent for efficient removal of hazardous dyes from industrial wastewater. J Water Process Eng. 2023;54:104054. doi:10.1016/J.JWPE.2023.104054
30. Zhou J, Tang C, Cheng B, Yu J, Jaroniec M. Rattle-type carbon-alumina core-shell spheres: Synthesis and application for adsorption of organic dyes. ACS Appl Mater Interfaces. 2012;4:2174–2179. doi:10.1021/AM300176K
31. Correa-Coyac D, Michtchenko A, Zacahua-Tlacuatl G, Cruz-Narváez Y, Castro-Arellano JJ, Sanpedro-Díaz M, et al. Adsorption and Photodegradation of Lanasol Yellow 4G in Aqueous Solution by Natural Zeolite Treated by CO2-Laser Radiation. Materials (Basel). 2023;16:4855. doi:10.3390/MA16134855
32. Ma Z, Zhang Q, Weng X, Mang C, Si L, Guan Z, et al. Fluoride ion adsorption from wastewater using magnesium(II), aluminum(III) and titanium(IV) modified natural zeolite: Kinetics, thermodynamics, and mechanistic aspects of adsorption. J Water Reuse Desalin. 2018;8:479–489. doi:10.2166/WRD.2017.037
33. Li CJ, Zhang YJ, Chen H, He PY, Meng Q. Development of porous and reusable geopolymer adsorbents for dye wastewater treatment. J Clean Prod. 2022;348:131278. doi:10.1016/J.JCLEPRO.2022.131278
34. Tariq R, Abatal M, Bassam A. Computational intelligence for empirical modeling and optimization of methylene blue adsorption phenomena using available local zeolites and clay of Morocco. J Clean Prod. 2022;370:133517. doi:10.1016/J.JCLEPRO.2022.133517
35. Shaban M, Abukhadra MR, Hamd A. Recycling of glass in synthesis of MCM-48 mesoporous silica as catalyst support for

Ni2O3 photocatalyst for Congo red dye removal. Clean Technol Environ Policy. 2018;20:13–28. doi:10.1007/S10098-017-1447-5
36. López-Rodríguez D, Micó-Vicent B, Jordán-Núñez J, Bonet-Aracil M, Bou-Belda E. Uses of Nanoclays and Adsorbents for Dye Recovery: A Textile Industry Review. Appl Sci 2021, Vol 11, Page 11422. 2021;11:11422. doi:10.3390/APP112311422
37. Orooji Y, Han N, Nezafat Z, Shafiei N, Shen Z, Nasrollahzadeh M, et al. Valorisation of nuts biowaste: Prospects in sustainable bio(nano)catalysts and environmental applications. J Clean Prod. 2022;347:131220. doi:10.1016/J.JCLEPRO.2022.131220
38. Li H, Li M, Zheng F, Wang J, Chen L, Hu P, et al. Efficient removal of water pollutants by hierarchical porous zeolite-activated carbon prepared from coal gangue and bamboo. J Clean Prod. 2021;325:129322. doi:10.1016/J.JCLEPRO.2021.129322
39. Yuan N, Zhao A, Hu Z, Tan K, Zhang J. Preparation and application of porous materials from coal gasification slag for wastewater treatment: A review. Chemosphere. 2022;287:132227. doi:10.1016/J.CHEMOSPHERE.2021.132227
40. Chai Z, Liu B, Lv P, Bai Y, Wang J, Song X, et al. Recycling of coal gasification fine slag as ultra-high capacity adsorbents for the removal of Rhodamine B dye: Graded synthesis method, kinetics and adsorption mechanism. Fuel. 2023;333:126318. doi:10.1016/J.FUEL.2022.126318
41. Mohammad Hosseini N, Sheshmani S, Shahvelayati AS, Ahmadi R, Adhami F. Development and Characterization of Environmentally-Friendly Magnetically Graphene Oxide-Embedded Chitosan as a Recyclable Heterogeneous Photocatalyst. J Polym Environ. 2024;32:1952–1971. doi:10.1007/S10924-023-03117-0
42. Slama H Ben, Chenari Bouket A, Pourhassan Z, Alenezi FN, Silini A, Cherif-Silini H, et al. Diversity of Synthetic Dyes from Textile Industries, Discharge Impacts and Treatment Methods. Appl Sci. 2021;11. doi:10.3390/app11146255
43. Katheresan V, Kansedo J, Lau SY. Efficiency of various recent wastewater dye removal methods: A review. J Environ Chem Eng. 2018;6:4676–97. doi:10.1016/J.JECE.2018.06.060
44. Mohammed L, Gomaa HG, Ragab D, Zhu J. Magnetic nanoparticles for environmental and biomedical applications: A review. Particuology. 2017;30:1–14. doi:10.1016/j.partic.2016.06.001
45. Ahmad T, Phul R, Khan H. Iron Oxide Nanoparticles: An Efficient Nano-catalyst. Curr Org Chem. 2019;23:994–1004. doi:10.2174/1385272823666190314153208
46. Adak L, Kundu D, Roy K, Saha M, Roy A. Reusable Iron/Iron Oxide-based Nanoparticles Catalyzed Organic Reactions. Curr Org Chem. 2022;26:399–417. doi:10.2174/1385272826666220209120545
47. Campos AFC, Michels-Brito PH, Da Silva FG, Gomes RC, Gomide G, Depeyrot J. Removal of direct yellow 12 from water using CTAB-coated core-shell bimagnetic nanoadsorbents. J Environ Chem Eng. 2019;7:103031. doi:10.1016/j.jece.2019.103031
48. Magomedov KE, Omelyanchik AS, Vorontsov SA, Čižmár E, Rodionova VV, Levada EV. SDS-Modified Iron Oxide Magnetic Nanoparticles for Removing of Methylene Blue from Aqueous Solution. Bull Russ Acad Sci Phys. 2023;87:720–727. doi:10.3103/S1062873823702027
49. Massart R. Preparation of aqueous magnetic liquids in alkaline and acidic media. IEEE Trans Magn. 1981;17:1247–8. doi:10.1109/TMAG.1981.1061188
50. Omelyanchik A, da Silva FG, Gomide G, Kozenkov I, Depeyrot J, Aquino R, et al. Effect of citric acid on the morpho-structural and magnetic properties of ultrasmall iron oxide nanoparticles. J Alloys Compd. 2021;883:160779. doi:10.1016/J.JALLCOM.2021.160779
51. Omelyanchik A, Kamzin AS, Valiullin AA, Semenov VG, Vereshchagin SN, Volochaev M, et al. Iron oxide nanoparticles synthesized by a glycine-modified coprecipitation method: Structure and magnetic properties. Colloids Surfaces A Physicochem Eng Asp. 2022;647:129090. doi:10.1016/J.COLSURFA.2022.129090
52. Scano A, Cabras V, Pilloni M, Ennas G. Microemulsions: The Renaissance of Ferrite Nanoparticle Synthesis. J Nanosci Nanotechnol. 2019;19:4824–4838. doi:10.1166/JNN.2019.16876
53. Muscas G, Peddis D, Cobianchi M, Lascialfari A, Cannas C, Musinu A, et al. Magnetic Interactions Versus Magnetic Anisotropy in Spinel Ferrite Nanoparticles. IEEE Magn Lett. 2019;10. doi:10.1109/LMAG.2019.2956908
54. Santoyo Salazar J, Perez L, De Abril O, Truong Phuoc L, Ihiawakrim D, Vazquez M, et al. Magnetic iron oxide nanoparticles in 10-40 nm range: Composition in terms of magnetite/maghemite ratio and effect on the magnetic properties. Chem Mater. 2011;23:1379–86. doi:10.1021/CM103188A
55. Synthesis of Superparamagnetic Iron Oxide Nanoparticles: SWOT Analysis Towards Their Conjugation to Biomolecules for Molecular Recognition Applications. J Nanosci Nanotechnol. 2019;19. doi:10.1166/jnn.2019.16931
56. Andrade ÂL, Fabris JD, Ardisson JD, Valente MA, Ferreira JMF. Effect of Tetramethylammonium Hydroxide on Nucleation, Surface Modification and Growth of Magnetic Nanoparticles. Francis LD, editor. J Nanomater. 2012;2012:454759. doi:10.1155/2012/454759
57. Abakumov MA, Semkina AS, Skorikov AS, Vishnevskiy DA, Ivanova A V., Mironova E, et al. Toxicity of iron oxide nanoparticles: Size and coating effects. J Biochem Mol Toxicol. 2018;32:e22225. doi:10.1002/JBT.22225
58. Eslamipour F, Hejazi P. Effects of surface modification and activation of magnetic nanoparticles on the formation of amylase immobilization bonds under different ionic strength conditions. J Mol Catal B Enzym. 2015;119:1–11. doi:10.1016/J.MOLCATB.2015.05.006
59. Jiang F, Li X, Zhu Y, Tang Z. Synthesis and magnetic characterizations of uniform iron oxide nanoparticles. Phys B Condens Matter. 2014;443:1–5. doi:10.1016/J.PHYSB.2014.03.009
60. Karaagac O, Kockar H, Tanrisever T. Properties of iron oxide nanoparticles synthesized at different temperatures. J Supercond Nov Magn. 2011;24:675–8. doi:10.1007/S10948-010-0932-4/METRICS
61. Nguyen DT, Park D-W, Kim K-S. Seed-Mediated Synthesis of Iron Oxide and Gold/Iron Oxide Nanoparticles. Jf Nanosci Nanotechnol. 2011. pp. 7214–7217. doi:10.1166/jnn.2011.4824
62. Aga-Tagieva SE, Omelyanchik AS, Magomedov KE, Motorzhina A V, Orudzhev FF, Rodionova V V, et al. PEGylated Iron-Oxide Nanoparticles: Structural, Magnetic, and Sorption Properties. Nanobiotechnology Reports. 2023;18:886–893. doi:10.1134/S2635167623600633
63. Corbett JF. Pseudo first-order kinetics. J Chem Educ. 1972;49:663. doi:10.1021/ED049P663
64. Robati D. Pseudo-second-orders kinetic equations for modeling adsorption systems for removal of lead ions using multi-walled carbon nanotube. J Nanostructure Chem. 2013;3:1–6. doi:10.1186/2193-8865-3-55
65. Kumar PS, Ramalingam S, Kirupha SD, Murugesan A, Vidhyadevi T, Sivanesan S. Adsorption behavior of nickel(II) onto cashew nut shell: Equilibrium, thermodynamics, kinetics, mechanism and process design. Chem Eng J. 2011;167. doi:10.1016/j.cej.2010.12.010
66. Alyasi H, Mackey H, McKay G. Adsorption of Methyl Orange from Water Using Chitosan Bead-like Materials. Mol 2023, Vol 28, Page 6561. 2023;28:6561. doi:10.3390/MOLECULES28186561
67. WeberJr. WJ, Morris JC. Kinetics of Adsorption on Carbon from Solution. J Sanit Eng Div. 1963;89:31–59. doi:10.1061/JSEDAI.0000430
68. Langmuir I. The adsorption of gases on plane surfaces of glass, mica and platinum. J Am Chem Soc. 1918;40. doi:10.1021/ja02242a004
69. Freundlich H. Über die Adsorption in Lösungen. Zeitschrift für Phys Chemie. 1907;57U:385–470. doi:10.1515/zpch-1907-5723

70. Temkin, M.J. Pyzhev V. Recent modifications to Langmuir isotherms, Acta Physiochim. Ussr 12. 1940;12:217–25.
71. Dubinin MM, Radushkevich LV. Equation of the characteristic curve of activated charcoal. Proc Acad Sci USSR Phys Chem Sect. 1947;55.
72. Li H, Jin H, Li R, Hua J, Zhang Z, Li R. Magnetic Fe3O4@SiO2 study on adsorption of methyl orange on nanoparticles. Sci Reports 2024 141. 2024;14:1–16. doi:10.1038/s41598-023-50368-x
73. Fisli A, Winatapura DS, Alfian A. The Surface Functionalization of Fe3O4 Nanoparticles by CTAB as Adsorbent for Methyl Orange Elimination in Water. J Phys Conf Ser. 2018;1091:012002. doi:10.1088/1742-6596/1091/1/012002
74. Munagapati VS, Yarramuthi V, Kim DS. Methyl orange removal from aqueous solution using goethite, chitosan beads and goethite impregnated with chitosan beads. J Mol Liq. 2017;240:329–339. doi:10.1016/J.MOLLIQ.2017.05.099
75. Khajeh M, Barkhordar A. Fe3O4/Graphene Oxide Composite for Adsorption of Methylene Blue and Methyl Orange in Water Treatment. J Appl Spectrosc. 2020;87:701–707. doi:10.1007/S10812-020-01057-4
76. Phi Y, Song G, Li A, Wang J, Wang H, Sun Y, et al. Graphene oxide-chitosan composite aerogel for adsorption of methyl orange and methylene blue: Effect of pH in single and binary systems. Colloids Surfaces A Physicochem Eng Asp. 2022;641:128595. doi:10.1016/J.COLSURFA.2022.128595
77. Barakat MA, Kumar R, Lima EC, Seliem MK. Facile synthesis of muscovite–supported Fe3O4 nanoparticles as an adsorbent and heterogeneous catalyst for effective removal of methyl orange: Characterisation, modelling, and mechanism. J Taiwan Inst Chem Eng. 2021;119:146–157. doi:10.1016/J.JTICE.2021.01.025
78. Zhao Y, Chen H, Li J, Chen C. Hierarchical MWCNTs/Fe3O4/PANI magnetic composite as adsorbent for methyl orange removal. J Colloid Interface Sci. 2015;450:189–195. doi:10.1016/J.JCIS.2015.03.015
79. Wu L, Liu X, Lv G, Zhu R, Tian L, Liu M, et al. Study on the adsorption properties of methyl orange by natural one-dimensional nano-mineral materials with different structures. Sci Rep. 2021 111. 2021;11:1–11. doi:10.1038/s41598-021-90235-1
80. Pang J, Han Q, Liu W, Shen Z, Wang X, Zhu J. Two basic bismuth nitrates: [Bi6O6(OH)2](NO3)4 · 2H2O with superior photodegradation activity for rhodamine B and [Bi6O5(OH)3](NO3)5 · 3H2O with ultrahigh adsorption capacity for methyl orange. Appl Surf Sci. 2017;422:283–294. doi:10.1016/J.APSUSC.2017.06.022
81. Siyasukh A, Chimupala Y, Tonanon N. Preparation of magnetic hierarchical porous carbon spheres with graphitic features for high methyl orange adsorption capacity. Carbon N Y. 2018;134:207–221. doi:10.1016/J.CARBON.2018.03.093

 DOI: 10.15826/chimtech.2024.11.3.05